



# CHORUS

This is the accepted manuscript made available via CHORUS. The article has been published as:

## Orbital Chern Insulator and Quantum Phase Diagram of a Kagome Electron System with Half-Filled Flat Bands

Yafei Ren, Hong-Chen Jiang, Zhenhua Qiao, and D. N. Sheng

Phys. Rev. Lett. **126**, 117602 — Published 18 March 2021

DOI: [10.1103/PhysRevLett.126.117602](https://doi.org/10.1103/PhysRevLett.126.117602)

# Orbital Chern Insulator and Quantum Phase Diagram of Kagome Electron System with Half-Filled Flat Bands

Yafei Ren,<sup>1,2</sup> Hong-Chen Jiang,<sup>3</sup> Zhenhua Qiao,<sup>1</sup> and D. N. Sheng<sup>2</sup>

<sup>1</sup>*ICQD, Hefei National Laboratory for Physical Sciences at Microscale, CAS Key Laboratory of Strongly-Coupled Quantum Matter Physics, and Department of Physics, University of Science and Technology of China, Hefei, Anhui 230026, China*

<sup>2</sup>*Department of Physics and Astronomy, California State University, Northridge, California 91330, USA*

<sup>3</sup>*Stanford Institute for Materials and Energy Sciences, SLAC National Accelerator Laboratory and Stanford University, Menlo Park, California 94025, USA*

(Dated: February 4, 2021)

We study the quantum phase diagram of electrons on kagome lattice with half-filled lowest flat bands by considering the antiferromagnetic Heisenberg interaction  $J$ , and short-range Coulomb interaction  $V$ . In the weak  $J$  regime, we identify a fully spin-polarized phase. The presence of finite  $V$  drives a spontaneous chiral current, which makes the system an orbital Chern insulator by contributing an orbital magnetization. Such an out-of-plane orbital magnetization allows the presence of a Chern insulating phase independent of the spin orientation in contrast to the spin-orbit coupling induced Chern insulator that disappears with in-plane ferromagnetism constrained by symmetry. Such a symmetry difference provides a criterion to distinguish the physical origin of topological responses in kagome systems. The orbital Chern insulator is robust against small coupling  $J$ . By further increasing  $J$ , we find that the ferromagnetic topological phase is suppressed, which first becomes partially-polarized and then enters a non-magnetic phase with **spin and charge nematicity**. The frustrated flat band allows the spin and Coulomb interaction to play an essential role in determining the quantum phases.

*Introduction*— The geometrical frustration of kagome lattice has attracted much attention in the past few decades [1–19]. At half filling, the frustration of antiferromagnetic spins can lead to quantum spin liquid phases and other exotic magnetic orders [1–3, 7–9]. Besides, the frustration of electronic hopping leads to a flat band that shows quadratic crossing with Dirac bands [20]. **At a semi-metallic filling with linear or quadratic Fermi point**, the presence of strong electronic interaction can open a band gap at the fermi points hosting nontrivial topology [21–33]. **Importantly, the flat band provides a platform to study the interaction driven exotic states with partial filling [6, 34–36].** Recently, theoretical calculations show that the (semi-)metallic flat bands can be achieved in realistic materials of kagome or kagome-like lattices [37–42], e.g., graphyne [40], where **interaction driven orbital magnetism and Chern insulator have been predicted at mean-field level**. In experiments, kagome lattices of transition metals have also been observed **contributed from various  $d$  orbitals near the Fermi level**, which provide novel platforms to investigate the intriguing physics from the interplay between strong repulsive interaction, magnetism, and topology [43–56].

The kagome lattices formed by transition metal atoms exhibit characteristic single-particle band structures, including quasi-two-dimensional Dirac bands [43–46] and flat bands near the Fermi energy [46–50]. Nontrivial band topology is observed by measuring anomalous Hall effect and orbital magnetic moments [43–47, 51–54]. These topological responses are closely related to the magnetic phases and strong electronic interactions as indicated by the experiments [43–45, 47, 54]. However, the role of

interaction, and its interplay with magnetism and topological band structure remain not clearly understood in kagome metal systems.

In this Letter, we theoretically investigate the interplay of topological phases and magnetism in the presence of strong correlation based on the extended  $t$ - $J$  model in Eq.(1) on kagome lattice with antiferromagnetic exchange interaction  $J$  and repulsive Coulomb interaction  $V$ . For electrons at the half-filling of the lowest flat bands, we identify three phases. At a small  $J$ , the short-range Coulomb interaction  $V$  drives a chiral current leading to spontaneous orbital magnetization and an energy gap hosting nonzero Chern number independent of the direction of the fully polarized spin. This distinguishes the orbital Chern insulator demonstrated here from the traditional one induced by spin-orbit coupling. Along with the increase of  $J$ , the system first undergoes a quantum phase transition to the partially spin-polarized phase and finally to the non-magnetic phase with **spin and charge nematic order stabilized by both  $J$  and  $V$** .

*Model and methods*— We consider a kagome lattice of spinful fermions described by an extended  $t$ - $J$  model with the Hamiltonian written as:

$$H = t \sum_{\langle ij \rangle, \alpha} c_{i, \alpha}^\dagger c_{j, \alpha} + J \sum_{\langle ij \rangle} (\mathbf{S}_i \cdot \mathbf{S}_j - \frac{1}{4} n_i n_j) + V_1 \sum_{\langle ij \rangle} n_i n_j + V_2 \sum_{\langle\langle ij \rangle\rangle} n_i n_j, \quad (1)$$

where  $c_{i, \alpha}^\dagger$  ( $c_{i, \alpha}$ ) is the creation (annihilation) operator of a fermion with spin  $\alpha = \{\uparrow, \downarrow\}$  at site  $i$  and  $n_i = \sum_{\alpha} c_{i, \alpha}^\dagger c_{i, \alpha}$  is the particle number operator.  $\mathbf{S}_i =$

$(S_i^x, S_i^y, S_i^z) = \frac{1}{2} \sum_{\alpha, \beta} c_{i, \alpha}^\dagger \sigma_{\alpha, \beta}^{x, y, z} c_{i, \beta}$  is the spin operator with  $\sigma^{x, y, z}$  being Pauli matrices. The hopping term  $t$  is set to be the energy unit, which makes the lowest energy band flat and quadratically touching with the middle one. The second term represents the exchange interaction with strength  $J > 0$  (antiferromagnetic type) between each pair of nearest neighbor sites. The third and fourth terms are the repulsive Coulomb interactions between electrons of first ( $\langle \dots \rangle$ ) and second ( $\langle \langle \dots \rangle \rangle$ ) nearest neighbors with strengths  $V_1$  and  $V_2$ , respectively. The Hilbert space is constrained by the no-double occupancy condition,  $n_i \leq 1$ , which corresponds to the on-site Hubbard interaction  $U = \infty$  limit.

We focus on the one-sixth filling case in a finite system of  $N_y \times N_x$  unit cells with total number of sites  $N_s = 3 \times N_y \times N_x$  and the number of fermions  $N_e = 2N_s/6$ . To illustrate the phase diagram, we set  $V_2$  as a fraction of  $V_1$  with  $V_1 = 2V_2 = V$  in our calculations and focus on the competition between interaction and  $J$  [29]. To characterize the ground states of the system with interactions, we employ the finite density matrix renormalization group (DMRG) algorithm [58–60] on cylinder geometry, where the boundary is open (periodic) along  $x$  ( $y$ )-direction, respectively. In DMRG calculations, we set  $N_y$  up to 4 unit cells (8 lattice sites) and keep the DMRG states up to  $M = 12000$  to guarantee a good convergence (with the truncation error smaller than  $10^{-5}$ ).

*Phase diagram*— As each spin component is conserved in our model, the ground states are calculated in sub-Hilbert space with total azimuthal spin  $S_z$  ranging from 0 to  $S_{max}$  with  $S_{max} = N_e/2$  (results are symmetric about positive and negative total  $S_z$ ). For a system of  $N_s = 3 \times 3 \times 4 = 36$ , we numerically calculate the ground-state energies for different  $S_z$  sector in the parameter space spanned by the short-range Coulomb interaction  $V$  and exchange interaction  $J$ . We identify three phases as shown in Fig. 1(a) according to the polarization of the ground state.

In phase-I, the system is fully spin-polarized, i.e., the ground states of different spin  $S_z$  ranging from  $-S_{max}$  to  $S_{max}$  are all degenerate with a total spin  $S = N_e/2$ . Our results suggest that the spontaneous ferromagnetization in this system is very strong, which can survive to finite antiferromagnetic coupling  $J \sim 0.4$ . Interestingly, an intermediate interaction strength  $V \sim 0.8$  can further enlarge the regime of the fully polarized phase, which may attribute to the enlarged energy gap by a larger  $V$ . As  $J$  increases, we find that the ferromagnetic phase is suppressed. For an intermediate  $J$ , the ground state jumps from  $S = N_e/2$  to a partially spin-polarized state with a smaller total  $S$  driven by antiferromagnetic coupling, which is illustrated as phase-II. The partially polarized phase also becomes excited states and the ground state lies in the spin sector of total  $S = 0$  labeled as phase-III in Fig. 1 for even larger  $J$ . [The changing of the color illustrates schematically the increase of the order param-](#)

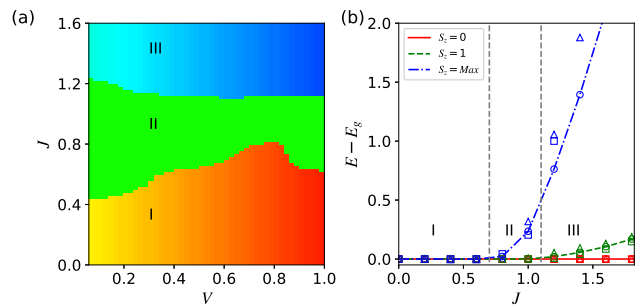


FIG. 1: (a) Phase diagram vs on-site repulsion-interaction strength  $V$  and exchange-interaction strength  $J$ . Phases I, II, and III are fully spin polarized spontaneous Chern insulator phase, partially polarized intermediate phase, and non-polarized phase with a rotation-symmetry breaking charge density wave, respectively. (b) Lowest energy level at each sector of azimuthal spin polarization  $S_z$  vs exchange-interaction strength  $J$  at  $V = 0.6$ . Circle, triangle, and square stand for the system with  $N_s = 36, 48$  and  $72$ , separately. The phase diagram is calculated for  $N_s = 3 \times 3 \times 4 = 36$  site system. The first and second nearest neighbor interactions are  $V_1 = 2V_2 = V$ . The dashed lines indicate the phase boundaries.

[eter with the increase of  \$V\$ , which plays an essential role in stabilizing phase-I and III \(see Supplemental Materials for more details\) \[57\].](#)

We further compare results from different system sizes to show the robustness of the quantum phase diagram. As shown in Fig. 1(b) at fixed  $V = 0.6$ , we present the energy difference  $E_g^{S_z} - E_g^0$  between ground state energy at different  $S_z = 0, 1, S_{max}$  as a function of  $J$ , for three different system sizes  $N_s = 3 \times 4 \times 3 = 36, 3 \times 4 \times 4 = 48$  and  $3 \times 3 \times 8 = 72$  sites, respectively. The same energy evolution with  $S_z$  is identified for these different systems. For a smaller  $J$ , the ground state has the total spin  $S = S_{max}$  with  $2S + 1$ -fold magnetic degeneracy, where the lowest energies in each  $S_z$  sector has the same energy. For  $J = 0.8$  in phase-II, the ground state has a smaller total spin  $S$  (i.e.,  $S < S_{max}$ ) since  $E_g^{S_{max}} - E_g^0 > 0$  while  $E_g^1 - E_g^0 = 0$ . For  $J > 1.0$  in Phase-III, both  $E_g^{S_{max}} - E_g^0 > 0$  and  $E_g^1 - E_g^0 > 0$ , so the ground state of the system has total spin  $S = 0$ .

The non-polarized phase-III is a non-magnetic insulator with [spin and charge nematicity](#). In Fig. 2(a), we plot the expectation value of electron number operator  $n_i$  at each site, where the circle size is proportional to the electron number  $\langle n_i \rangle$ . One can find that the charge densities for different sublattices are imbalanced, where A and B sites show similar densities, which are much larger than that of sublattice C. The intra-unit cell charge density difference  $\delta n_i = n_{A,i} - n_{C,i}$  at  $i$ th unit cell is plotted as a function of the unit cell position  $i_x$  in the inset of Fig. 2(b). The charge imbalance away from the boundaries shows weak spatial dependence. In the middle of the system, we can see that such a charge-density pattern

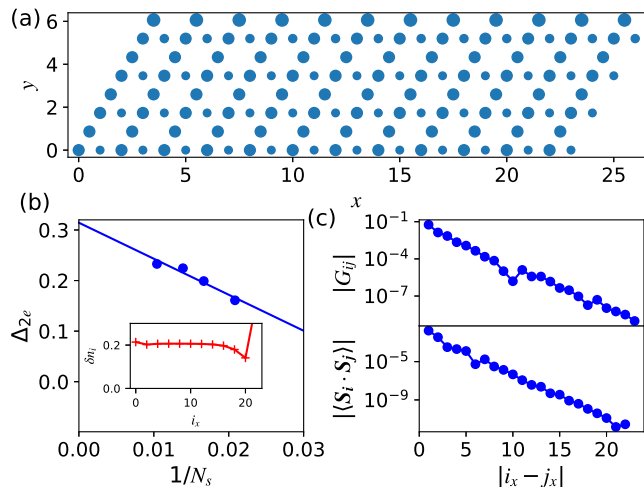


FIG. 2: Measurements of ground states in phase region III with  $J = 1.5$  and  $V = 0.5$ . (a) Charge density at each site. Circle size represents the magnitude of density. (b) Scaling behavior of the charge gap. Inset: intra-unit cell charge density imbalance  $\delta n_i$  as the unit-cell position along  $x$  direction  $i_x$ . (c) Dependence of electron hopping function  $G_{ij}$  and spin-spin correlation between two sites on their distance.

preserves the translation symmetry of the system while breaks the rotation symmetry leading to the nematicity. We have checked that such density and spin patterns are robust against the width  $L_y$  of the cylinders, **by lowering the spin and interaction energy**. The insulating nature of this phase is characterized by a finite charge excitation gap defined as  $\Delta_{2e} = E_g^0(N_e + 2) + E_g^0(N_e - 2) - 2E_g^0(N_e)$  which is calculated in the ground state  $S_z = 0$  spin sector by adding/removing two electrons (one spin up and one spin down). The scaling behavior of the charge gap as a function of  $1/N_s$  is plotted in Fig. 2(b), where one can find that the charge gap is finite in thermodynamic limit suggesting the system is an insulator.

Since  $J$  represents the strength of the antiferromagnetic coupling, we also check if there is any magnetic order. We show that the state is non-magnetic due to the small site filling number where the antiferromagnetic coupling becomes less efficient. The spin-spin correlation  $|\langle \mathbf{S}_i \cdot \mathbf{S}_j \rangle|$  decreases exponentially as a function of the distance between two sites as shown in the lower panel of Fig. 2(c), where the correlation between sites  $i$  and  $j$  with the same  $y$  coordinate is plotted as a function of their distance  $i_x - j_x$  along  $x$ -direction. **Nevertheless, the spin-spin correlation between the nearest neighboring sites shows nematicity that further lowers the total energy [57].** We also study the electron hopping function  $G_{ij} \equiv \langle c_i^\dagger c_j \rangle$  as shown in the upper panel of Fig. 2(c) where the magnitude of  $G_{ij}$  also decreases exponentially as the distance increases, being consistent with a charge insulator state.

The partially polarized phase-II shows a spin polarization close to the fully polarized state [57] with flipped

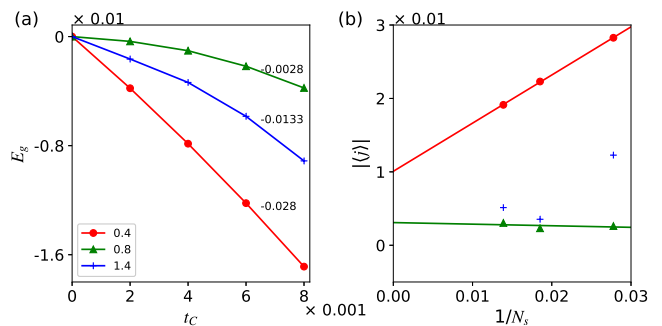


FIG. 3: (a) Variation of ground state energy due to the presence of nonzero  $t_C$  at different  $J$  for  $N_s = 36$  sites. The slope of each curve at  $t_C = 0$  represents the average current  $\langle j \rangle$  of the system as labelled by the number nearby. (b) Size scaling of current at the corresponding  $J$ . The repulsion interaction  $V = 0.6$  here.

spins appear at the boundary of the system. To understand if such a phase can extend to intermediate spin polarization, larger systems are required, which is beyond our current simulation capability.

*Spontaneous chiral current*— We now turn to Phase-I where the system is fully spin-polarized. Our result is complementary to the kinetic ferromagnetism in Ref. 6 that is insensitive to the sign of hopping energy and focus on the regime of  $|t| \ll V$ . Besides, the weak  $J$  limit corresponds to a large  $U$  and the ferromagnetic ground state agrees with the graph-theory analysis of  $t$ - $U$  model on kagome lattice with Hubbard  $U > 0$  [62]. In the following, we reveal the nontrivial orbital effect and electronic topology besides the ferromagnet when the Coulomb interaction beyond on-site Hubbard  $U$  is included.

Here, we demonstrate the spontaneous chiral currents appear in the ferromagnetic phase of the spinful model in the presence of finite  $V$ . We consider a chiral-symmetry-breaking hopping term  $h_C = i\chi t_C \sum_{\langle ij \rangle, \alpha} c_{i, \alpha}^\dagger c_{j, \alpha}$  as a perturbation, where  $t_C \ll t = 1$  is small and  $\chi = \pm 1$  when the electron hopping is clockwise/anti-clockwise in each triangle. We can then detect the loop current following the Hellmann-Feynman theorem [31, 63, 64] via

$$\langle j \rangle = \frac{1}{2N_s} \frac{\partial E(t_C)}{\partial t_C} \Big|_{t_C \rightarrow 0}, \quad (2)$$

where  $E(t_C) = \langle \Psi | H(h_C) | \Psi \rangle$  with  $|\Psi\rangle$  being the ground state of the system and  $N_s$  is the number of sites. In Fig. 3(a), we show the ground state energy difference  $E_g^0(t_C) - E_g^0(t_C = 0)$  as a function of  $t_C$  for  $N_s = 36$  with  $J = 0, 4, 0.8$ , and  $1.4$  representing three different phases, respectively. One can find that in the ferromagnetic region, the ground state energy decreases linearly as a function of  $t_C$  (we use small  $t_C$  up to 0.008) corresponding to a loop current of  $j = 0.028$  for each triangle. The constant current at weak  $J$  is robust against the system size  $N_s$ , as shown in Fig. 3(b) where the scaling behavior of the current as a function of  $1/N_s$  is plotted by the red

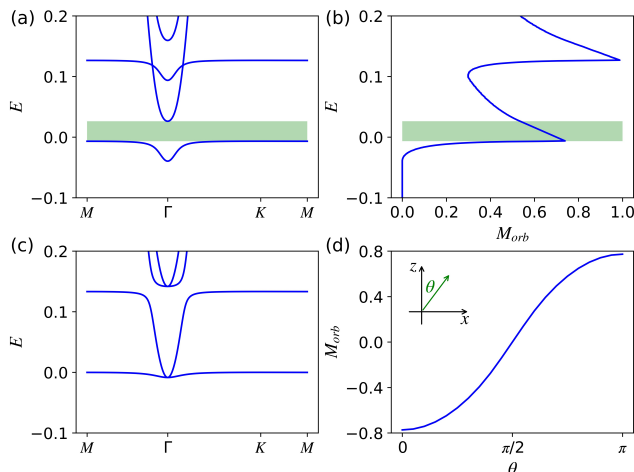


FIG. 4: (a)-(b) Electronic band structure and orbital magnetization in the presence of spontaneous chiral current and ferromagnetism. (b) Orbital magnetization vs chemical potential. Green shaded region shows the band gap. **Unit of magnetization:**  $\frac{et}{(2\pi)^2\hbar}$ . (c)-(d) Band structure and orbital magnetization in the presence of Kane-Mele type spin-orbit coupling and ferromagnetism. (d) Orbital magnetization vs azimuthal angle  $\theta$  that characterizes the spin orientation as illustrated in the inset.

line with solid circles. We find that the current is finite in the order of  $10^{-2}$  at the large  $N_s$  limit, suggesting the existence of finite current in the thermodynamic limit. The finite current supports the quantum anomalous Hall effect for phase-I with nonzero  $V$ .

For partially polarized and nonmagnetic phases with  $J = 0.8$  and  $J = 1.4$ , the ground state energies decrease near quadratically with  $t_C$  as shown in Fig. 3(a). For  $J = 0.8$ , the current keeps a small value whereas the current drops a lot at  $J = 1.4$  as  $N_s$  increases. We caution that because of the quadratic behavior of currents for phase region II and III, we will see much reduced or vanishing current if we take the small  $t_C$  limit, which is negligible as it is related to an energy difference at the same order as the relative error in DMRG.

*Spontaneous orbital magnetization*— The spontaneous chiral current will manifest itself by a nonzero spontaneous orbital magnetization. In the presence of nonzero loop current, the mean-field electronic structure is plotted in Fig. 4(a), which is independent of the spin orientation and exhibits a band gap as labeled by the shadow region. When the chemical potential lies in the band gap at  $1/6$  filling, nonzero out-of-plane orbital magnetization  $M_{orb}$  appears as shown in Fig. 4(b) [57]. Inside the gap, the linear dependence of  $M_{orb}$  on chemical potential is attributed to the chiral edge state of the Chern insulator. **The corresponding magnetic moment per unit cell is  $\mu_B \frac{2m_e}{m^*}$  where the  $m_e$  is the mass of electron and the effective mass  $m^* = \frac{(2\pi\hbar)^2}{tA_u}$  is defined by the energy unit  $t$  and the unit cell area  $A_u$ . By employing the typical hop-**

ping energy  $t \sim 0.5$  eV and lattice constant  $a \sim 0.5$  nm of kagome lattice in kagome metal [46], the corresponding magnetic moment per unit cell is about  $0.05 \mu_B$ . This makes the spontaneous Chern insulator an orbital magnet independent of the spin polarization.

In contrast, for the topological phase induced by spin-orbit coupling, the band topology and the associated orbital magnetization show strong dependence on the spin orientation [57]. In the presence of the symmetry-allowed Kane-Mele type spin-orbit coupling [57] in a planar kagome lattice, the in-plane ferromagnetism (the azimuthal angle  $\theta = \pi/2$ ) cannot open a band gap as shown in Fig. 4(c). Thus, in the absence of chiral current, the system is topologically trivial with in-plane ferromagnetism, which is constrained by the symmetry. The corresponding orbital magnetization is also zero as shown in Fig. 4(d) where the orbital magnetization is plotted as function of the spin orientation in the presence of only spin-orbit coupling and ferromagnetism. One can find that both the magnitude and the sign of the orbital magnetization depend strongly on the spin-orientation  $\theta$ .

*Summary and discussion*— We have demonstrated the quantum phase diagram of an electronic kagome lattice with half-filled lowest flat-band by considering the interplay between the short-range Coulomb interaction  $V$  and the nearest neighbor antiferromagnetic Heisenberg interaction  $J$ . In the large  $J$  limit, the system is a non-magnetic insulator with **spin and charge nematicity**. **The Coulomb interaction  $V$  plays an essential role to stabilize this phase in the presence of flat band with frustrated kinetic energy**. As  $J$  decreases gradually, the system becomes partially polarized first. In the weak  $J$  regime, the system exhibits a fully spin-polarized ferromagnetic phase. The short-ranged Coulomb interaction  $V$  drives the formation of spontaneous chiral current, which manifests itself as an orbital magnet. The orbital magnetization points out of plane that is also independent of the spin polarization. This provides another example for the presence of orbital magnet independent of the spin polarization besides the magic-angle twisted bilayer graphene [66–68].

Such out-of-plane orbital magnetization breaks the mirror symmetries and thus allows the presence of an orbital Chern insulator, which is independent of the spin polarization. In contrast, the Chern insulator induced by spin-orbit coupling shows a strong dependence on the spin polarization, which disappears when the polarization lies in-plane constrained by symmetry. Our work provides a way to distinguish these two types of Chern insulators for realistic materials.

*Acknowledgments*.— Y.R. and Z.Q. acknowledge the financial support from the National Key R & D Program (No. 2017YFB0405703), NNSFC (No. 11974327), Fundamental Research Funds for the Central Universities, and Anhui Initiative in Quantum Information Technologies. This material is based upon work supported

by the U.S. Department of Energy, Office of Science, Advanced Scientific Computing Research and Basic Energy Sciences, Materials Sciences and Engineering Division, Scientific Discovery through Advanced Computing (SciDAC) program under the grant number DE-AC02-76SF00515 (HCJ,DNS).

- 
- [1] L. Savary and L. Balents, Quantum spin liquids: a review, *Rep. Prog. Phys.* **80** 016502 (2017).
- [2] Yi Zhou, Kazushi Kanoda, and Tai-Kai Ng, Quantum spin liquid states, *Rev. Mod. Phys.* **89**, 025003 (2017).
- [3] C. Broholm, R. J. Cava, S. A. Kivelson, D. G. Nocera, M. R. Norman, and T. Senthil, Quantum spin liquids, *Science* **367**, eaay0668 (2020).
- [4] R. W. Smaha, W. He, J. M. Jiang, *et al.*, Materializing rival ground states in the barlowite family of kagome magnets: quantum spin liquid, spin ordered, and valence bond crystal states. *npj Quantum Mater.* **5**, 23 (2020).
- [5] N. J. Ghimire and I. I. Mazin, Topology and correlations on the kagome lattice, *Nat. Mater.* **19**, 137 (2020).
- [6] F. Pollmann, P. Fulde, and K. Shtengel, Kinetic Ferromagnetism on a Kagome Lattice, *Phys. Rev. Lett.* **100**, 136404 (2008).
- [7] H. C. Jiang, Z. Y. Weng, and D. N. Sheng, Density Matrix Renormalization Group Numerical Study of the Kagome Antiferromagnet, *Phys. Rev. Lett.* **101**, 117203 (2008).
- [8] H. C. Jiang, Z. Wang, and L. Balents, Identifying Topological Order by Entanglement Entropy, *Nature Physics* **8**, 902 (2012).
- [9] S.-S. Gong, W. Zhu, L. Balents, and D. N. Sheng, Global phase diagram of competing ordered and quantum spin-liquid phases on the kagome lattice, *Phys. Rev. B* **91**, 075112 (2015).
- [10] X. Plat, F. Alet, S. Capponi, and K. Totsuka, Magnetization plateaus of an easy-axis kagome antiferromagnet with extended interactions, *Phys. Rev. B* **92**, 174402 (2015).
- [11] H.-M. Guo and M. Franz, Topological insulator on the kagome lattice, *Phys. Rev. B* **80**, 113102 (2009).
- [12] S.-L. Yu and J.-X. Li, Chiral superconducting phase and chiral spin-density-wave phase in a Hubbard model on the kagome lattice, *Phys. Rev. B* **85**, 144402 (2014).
- [13] M. L. Kiesel, C. Platt, and R. Thomale, Unconventional Fermi Surface Instabilities in the Kagome Hubbard Model, *Phys. Rev. Lett.* **110**, 126405 (2013).
- [14] Se Kwon Kim and J. Zang, U(1) symmetry of the spin-orbit coupled Hubbard model on the kagome lattice, *Phys. Rev. B* **92**, 205106 (2015).
- [15] S. Guertler, Kagome lattice Hubbard model at half filling, *Phys. Rev. B* **90**, 081105(R) (2014).
- [16] R. Higa and K. Asano, Bond formation effects on the metal-insulator transition in the half-filled kagome Hubbard model, *Phys. Rev. B* **93**, 245123 (2016).
- [17] S. Guertler and H. Monien, Unveiling the Physics of the Doped Phase of the  $t$ - $J$  Model on the Kagome Lattice, *Phys. Rev. Lett.* **111**, 097204 (2013).
- [18] W.-S. Wang, Z.-Z. Li, Y.-Y. Xiang, and Q.-H. Wang, Competing electronic orders on kagome lattices at van Hove filling, *Phys. Rev. B* **87**, 115135 (2013).
- [19] M. Maksymenko, R. Moessner, and K. Shtengel, Persistence of the flat band in a kagome magnet with dipolar interactions, *Phys. Rev. B* **96**, 134411 (2017).
- [20] Doron L. Bergman, Congjun Wu, and Leon Balents, *Phys. Rev. B* **78**, 125104 (2008).
- [21] K. Sun, H. Yao, E. Fradkin, and S. A. Kivelson, Topological Insulators and Nematic Phases from Spontaneous Symmetry Breaking in 2D Fermi Systems with a Quadratic Band Crossing, *Phys. Rev. Lett.* **103**, 046811 (2009).
- [22] K. Sun, W. Vincent Liu, A. Hemmerich, and S. Das Sarma, Topological semimetal in a fermionic optical lattice, *Nat. Phys.* **8**, 67 (2012).
- [23] J. Wen, A. Rüegg, C.-C. Joseph Wang, and G. A. Fiete, Interaction-driven topological insulators on the kagome and the decorated honeycomb lattices, *Phys. Rev. B* **82**, 075125 (2010).
- [24] Q. Liu, H. Yao, and T. Ma, Spontaneous symmetry breaking in a two-dimensional kagome lattice, *Phys. Rev. B* **82**, 045102 (2010).
- [25] F. Pollmann, K. Roychowdhury, C. Hotta, and K. Penc, Interplay of charge and spin fluctuations of strongly interacting electrons on the kagome lattice, *Phys. Rev. B* **90**, 035118 (2014).
- [26] K. Ferhat and A. Ralko, Phase diagram of the 1/3-filled extended Hubbard model on the kagome lattice, *Phys. Rev. B* **89**, 155141 (2014).
- [27] W.-F. Tsai, C. Fang, H. Yao, and J. Hu, Interaction-driven topological and nematic phases on the Lieb lattice, *New J. Phys.* **17**, 055016 (2015).
- [28] W. Zhu, S.-S. Gong, T.-S. Zeng, L. Fu, and D. N. Sheng, Interaction-Driven Spontaneous Quantum Hall Effect on a Kagome Lattice, *Phys. Rev. Lett.* **117**, 096402 (2016).
- [29] Y. Ren, T.-S. Zeng, W. Zhu, and D. N. Sheng, Quantum anomalous Hall phase stabilized via realistic interactions on a kagome lattice, *Phys. Rev. B* **98**, 205146 (2018).
- [30] S. Sur, S.-S. Gong, K. Yang, and O. Vafek, Quantum anomalous Hall insulator stabilized by competing interactions, *Phys. Rev. B* **98**, 125144 (2018).
- [31] T. Zeng, W. Zhu, and D. Sheng, Tuning topological phase and quantum anomalous Hall effect by interaction in quadratic band touching systems, *npj Quant. Mater.* **3**, 49 (2018).
- [32] H.-Y. Hui, M. Chen, S. Tewari, and V. W. Scarola, Chiral topological phases in optical lattices without synthetic fields, *Phys. Rev. A* **98**, 023609 (2018).
- [33] S. Ray, M. Vojta, and L. Janssen, Soluble Fermionic Quantum Critical Point in Two Dimensions, [arXiv:2001.09155](https://arxiv.org/abs/2001.09155).
- [34] Congjun Wu, Orbital Analogue of the Quantum Anomalous Hall Effect in  $p$ -Band Systems, *Phys. Rev. Lett.* **101**, 186807 (2008).
- [35] C. Wu, D. Bergman, L. Balents, and S. Das Sarma, Flat Bands and Wigner Crystallization in the Honeycomb Optical Lattice, *Phys. Rev. Lett.* **99**, 070401 (2007).
- [36] C. Wu and S. Das Sarma,  $p_{x,y}$ -orbital counterpart of graphene: Cold atoms in the honeycomb optical lattice, *Phys. Rev. B* **77**, 235107 (2008).
- [37] S. Baidya, S. Kang, C. H. Kim, and J. Yu, Chern insulator with a nearly flat band in the metal-organic-framework-based Kagome lattice, *Sci. Rep.* **9**, 13807 (2019).
- [38] W. Jiang, Z. Liu, J.-W. Mei, B. Cui, and F. Liu, Tunable Bi-frustrated Electron Spin and Charge States in

- a Cu-Hexaaminobenzene Framework, *Nanoscale* **11**, 955 (2019).
- [39] Z. Li, J. Zhuang, L. Wang, H. Feng, Q. Gao, X. Xu, W. Hao, X. Wang, C. Zhang, K. Wu, S. X. Dou, L. Chen, Z. Hu, and Y. Du, Realization of flat band with possible nontrivial topology in electronic Kagome lattice, *Science Advances* **4**, eaau4511 (2018).
- [40] Y. Chen, S. Xu, Y. Xie, C. Zhong, C. Wu, and S. B. Zhang, Ferromagnetism and Wigner crystallization in kagome graphene and related structures, *Phys. Rev. B* **98**, 035135 (2018).
- [41] J.-Y. You, B. Gu, and G. Su, Flat Band and Hole-induced Ferromagnetism in a Novel Carbon Monolayer, *Scientific Reports* **9**, 20116 (2019).
- [42] W. H. Han, S. Kim, I.-H. Lee, and K. J. Chang, A Metal-Insulator Transition via Wigner Crystallization in Boron Triangular Kagome Lattice, arXiv:1902.08390.
- [43] L. Ye, M. Kang, J. Liu, F. von Cube, C. R. Wicker, T. Suzuki, C. Jozwiak, A. Bostwick, E. Rotenberg, D. C. Bell, L. Fu, R. Comin, and J. G. Checkelsky, Massive Dirac fermions in a ferromagnetic kagome metal, *Nature* **555**, 638 (2018).
- [44] L. Ye, M. K. Chan, R. D. McDonald, D. Graf, M. Kang, J. Liu, T. Suzuki, R. Comin, L. Fu, and J. G. Checkelsky, de Haas-van Alphen effect of correlated Dirac states in kagome metal  $\text{Fe}_3\text{Sn}_2$ , *Nat. Commun.* **10**, 4870 (2019).
- [45] J.-X. Yin, S. S. Zhang, H. Li, K. Jiang, G. Chang, B. Zhang, B. Lian, C. Xiang, I. Belopolski, H. Zheng, T. A. Cochran, S.-Y. Xu, G. Bian, K. Liu, T.-R. Chang, H. Lin, Z.-Y. Lu, Z. Wang, S. Jia, W. Wang, and M. Z. Hasan, Giant and anisotropic many-body spin-orbit tunability in a strongly correlated kagome magnet, *Nature* **562**, 91 (2018).
- [46] M. Kang, L. Ye, S. Fang, J.-S. You, A. Levitan, M. Han, J. I. Facio, C. Jozwiak, A. Bostwick, E. Rotenberg, M. K. Chan, R. D. McDonald, D. Graf, K. Kaznatcheev, E. Vescovo, D. C. Bell, E. Kaxiras, J. van den Brink, M. Richter, M. Prasad Ghimire, J. G. Checkelsky, and R. Comin, Dirac fermions and flat bands in the ideal kagome metal  $\text{FeSn}$ , *Nature Materials* **19**, 163 (2020).
- [47] J.-X. Yin, S. S. Zhang, G. Chang, Q. Wang, S. S. Tsirkin, Z. Guguchia, B. Lian, H. Zhou, K. Jiang, I. Belopolski, N. Shumiya, D. Multer, M. Litskevich, T. A. Cochran, H. Lin, Z. Wang, T. Neupert, S. Jia, H. Lei, and M. Zahid Hasan, Negative flat band magnetism in a spin-orbit-coupled correlated kagome magnet, *Nature Physics* **15**, 443 (2019).
- [48] B. C. Sales, J. Yan, W. R. Meier, A. D. Christianson, S. Okamoto, and M. A. McGuire, 3D electronic, 2D in-plane AFM Electronic, magnetic, and thermodynamic properties of the kagome layer compound  $\text{FeSn}$ , *Phys. Rev. Materials* **3**, 114203 (2019).
- [49] T. Y. Yang, Q. Wan, Y. H. Wang, M. Song, J. Tang, Z. W. Wang, H. Z. Lv, N. C. Plumb, M. Radovic, G. W. Wang, G. Y. Wang, Z. Sun, R. Yu, M. Shi, Y. M. Xiong, and N. Xu, Evidence of orbit-selective electronic kagome lattice with planar flat-band in correlated paramagnetic  $\text{YCr}_6\text{Ge}_6$ , arXiv:1906.07140
- [50] Z. Liu, M. Li, Q. Wang, G. Wang, C. H. P. Wen, K. Jiang, X. Lu, S. Yan, Y. Huang, D. Shen, J. Yin, Z. Wang, Z. Yin, H. Lei, and S. Wang, Orbital-Selective Dirac Fermions and Extremely Flat Bands in the Non-magnetic Kagome Metal  $\text{CoSn}$ , arXiv:2001.11738.
- [51] E. Liu, Y. Sun, N. Kumar, L. Muechler, A. Sun, L. Jiao, S.-Y. Yang, D. Liu, A. Liang, Q. Xu, J. Kroder, V. Sü, H. Borrmann, C. Shekhar, Z. Wang, C. Xi, W. Wang, W. Schnelle, S. Wirth, Y. Chen, S. T. B. Goennenwein, and C. Felser, Giant anomalous Hall effect in a ferromagnetic kagome-lattice semimetal, *Nature Physics* **14**, 1125-1131 (2018).
- [52] Q. Wang, Y. Xu, R. Lou, Z. Liu, M. Li, Y. Huang, D. Shen, H. Weng, S. Wang, and Hechang Lei, Large intrinsic anomalous Hall effect in half-metallic ferromagnet  $\text{Co}_3\text{Sn}_2\text{S}_2$  with magnetic Weyl fermions, *Nat. Commun.* **9**, 3681 (2018).
- [53] J. Shen, Q. Zeng, S. Zhang, W. Tong, L. Ling, C. Xi, Z. Wang, E. Liu, W. Wang, G. Wu, and B. Shen, On the anisotropies of magnetization and electronic transport of magnetic Weyl semimetal  $\text{Co}_3\text{Sn}_2\text{S}_2$ , *Appl. Phys. Lett.* **115**, 212403 (2019).
- [54] E. Lachman, R. A. Murphy, N. Maksimovic, R. Kealhofer, S. Haley, R. D. McDonald, J. R. Long, and J. G. Analytis, Exchange biased anomalous Hall effect driven by frustration in a magnetic kagome lattice, *Nature Communications* **11**, 560 (2020).
- [55] Y. Li, Q. Wang, L. D. Schmitt, Z. Guguchia, R. D. Desautels, J.-X. Yin, Q. Du, W. Ren, X. Zhao, Z. Zhang, I. A. Zaliznyak, C. Petrovic, W. Yin, M. Zahid Hasan, H. Lei, and J. M. Tranquada, Magnetic-Field Control of Topological Electronic Response near Room Temperature in Correlated Kagome Magnets, *Phys. Rev. Lett.* **123**, 196604 (2019).
- [56] Z. Guguchia, J. A. T. Verezhak, D. J. Gawryluk, S. S. Tsirkin, J.-X. Yin, I. Belopolski, H. Zhou, G. Simutis, S.-S. Zhang, T. A. Cochran, G. Chang, E. Pomjakushina, L. Keller, Z. Skrzeczowska, Q. Wang, H. C. Lei, R. Khasanov, A. Amato, S. Jia, T. Neupert, H. Luetkens, and M. Z. Hasan, Tunable anomalous Hall conductivity through volume-wise magnetic competition in a topological kagome magnet, *Nat. Commun.* **11**, 559 (2020).
- [57] See Supplemental Material for a detailed discussion on the spin and charge nematicity in phase-III, the spin polarization of the ground states at different spin sectors in phase-II, calculation of orbital magnetization band topology of kagome lattice with spin-orbit coupling and ferromagnetism, and role of Zeeman field.
- [58] S. R. White, Density matrix formulation for quantum renormalization groups, *Phys. Rev. Lett.* **69**, 2863 (1992).
- [59] I. P. McCulloch, Infinite size density matrix renormalization group, revisited, arXiv:0804.2509.
- [60] S. S. Gong, W. Zhu, and D. N. Sheng, Emergent Chiral Spin Liquid: Fractional Quantum Hall Effect in a Kagome Heisenberg Model, *Sci. Rep.* **4**, 6317 (2014).
- [61] W. Zhu, S. S. Gong, F. D. M. Haldane, and D. N. Sheng, Topological characterization of the non-Abelian Moore-Read state using density-matrix renormalization group, *Phys. Rev. B* **92**, 165106 (2015).
- [62] A. Mielke, Exact ground states for the Hubbard model on the Kagome lattice, *J. Phys. A: Math. Gen.* **25**, 4335 (1992).
- [63] H. Hellmann, Einführung in Die Quantenchemie. (Deuticke, Leipzig, 1937).
- [64] R. P. Feynman, Forces in molecules. *Phys. Rev.* **56**, 340 (1939).
- [65] Y. Ren, J. Zeng, X. Deng, F. Yang, H. Pan, and Z. Qiao, Quantum anomalous Hall effect in atomic crystal layers from in-plane magnetization, *Phys. Rev. B* **94**, 085411

- (2016).
- [66] X. Lu, P. Stepanov, W. Yang, M. Xie, M. A. Aamir, I. Das, C. Urgell, K. Watanabe, T. Taniguchi, G. Zhang, A. Bachtold, A. H. MacDonald, D. K. Efetov, Superconductors, orbital magnets and correlated states in magic-angle bilayer graphene. *Nature* 574, **653**-657 (2019).
- [67] J. Zhu, J.-J. Su, A. H. MacDonald, The Curious Magnetic Properties of Orbital Chern Insulators, arXiv:2001.05084v4.
- [68] H. Polshyn, J. Zhu, M. A. Kumar, Y. Zhang, F. Yang, C. L. Tschirhart, M. Serlin, K. Watanabe, T. Taniguchi, A. H. MacDonald, and A. F. Young, Nonvolatile switching of magnetic order by electric fields in an orbital Chern insulator, arXiv:2004.11353.